Biosensors and Bioelectronics 60 (2014) 161–166

Contents lists available at ScienceDirect

Biosensors and Bioelectronics

journal homepage: www.elsevier.com/locate/bios

Short communication

Tryptamine functionalized reduced graphene oxide for label-free DNA impedimetric biosensing

Zhao Zhang [a], Liqiang Luo [a,*], Guifang Chen [b], Yaping Ding [a], Dongmei Deng [a], Chunhai Fan [c]

[a] College of Sciences, Shanghai University, Shanghai 200444, PR China
[b] Laboratory of Biosensing Technology, School of Life Sciences, Shanghai University, Shanghai 200444, PR China
[c] Division of Physical Biology and Bioimaging Center, Shanghai Synchrotron Radiation Facility, Shanghai Institute of Applied Physics, Chinese Academy of Sciences, Shanghai 201800, PR China

ARTICLE INFO

Article history:
Received 6 January 2014
Received in revised form
13 March 2014
Accepted 31 March 2014
Available online 18 April 2014

Keywords:
Reduced graphene oxide
Tryptamine
Electrochemical impedance
DNA biosensor

ABSTRACT

A novel simple protocol of synthesizing tryptamine-functionalized reduced graphene oxide (TRA–rGO) was proposed to fabricate label-free electrochemical impedance DNA biosensor. TRA was anchored to rGO with its indole ring via π-stacking interaction. The morphology, conductivity and interaction of TRA–rGO were characterized by atomic force microscopy, high resolution transmission electron microscopy, cyclic voltammetry, electrochemical impedance spectroscopy (EIS) as well as Raman and fluorescence spectroscopy. The amino-substituted oligonucleotide probe was conjugated to TRA by cross-linker glutaraldehyde for preparing an electrochemical biosensing platform. The DNA hybridization reaction of oligonucleotide probe with target DNA was monitored by EIS. Under optimum conditions, the proposed biosensor exhibited high sensitivity and low detection limit for detecting complementary oligonucleotide. The target oligonucleotide could be quantified in a wide range of 1.0×10^{-12}–1.0×10^{-7} M with low detection limit of 5.2×10^{-13} M ($S/N=3$).

1. Introduction

Graphene, a two-dimensional monolayer carbon material isolated by mechanically peeling off graphite crystals in 2004, shows many intriguing thermal, electric and mechanical properties (Dutta and Pati, 2010; Meyer et al., 2007; Novoselov et al., 2004, Rao et al., 2009; Wang et al., 2011). However, graphene tends to form irreversible agglomerates or even stack to graphite through π-stacking and Van der Waals interactions (Li et al., 2008). Therefore, prevention of aggregation is important in the preparation and processing of graphene. Covalent (Sun et al., 2010; Yang et al., 2011) or non-covalent (Ramanathan et al., 2008; Wen et al., 2011; Zhang et al., 2012) functionalization approaches have been developed for the stabilization and modification of graphene. Thereinto, non-covalent functionalization of graphene based on π-stacking interaction in hybrid structures (Artiles et al., 2011; Premkumar and Geckeler, 2012) has less destructive impact on its structure and electronic network, thus improving the hydrophilicity (Ghosh et al., 2010; Xu et al., 2008) and preserving its unique properties such as high specific surface area, rapid heterogeneous electron transfer, great mechanical strength and biocompatibility (Chen, 2013; Liu et al., 2012; Su et al., 2009).

Tryptamine (TRA), a common low-cost reagent in organic synthesis field, is one of the prototypical flexible biogenic amines (Hayama et al., 2012; Pham et al. 2012). Here, TRA is chosen to non-covalently functionalize reduced graphene oxide (rGO) because it can irreversibly anchor to the large hydrophobic surface of rGO via its indole ring by π-stacking interaction (Rajesh et al., 2009), which is the same as guanine-functionalized graphene nanoribbons (Tang et al., 2012) and 1-aminopyrene-functionalized multiwalled carbon nanotubes (Wang et al., 2008a). The simple and cost-effective preparation process of TRA-functionalized rGO (TRA–rGO) does not need expensive chemicals or corrosive acids and can preserve the integrity and the electronic structure of rGO (Liu et al., 2012).

DNA biosensors are currently an area of tremendous interest due to their advantages of simplicity, speed and economy in gene analysis (Liu et al., 2013; Lin et al., 2013). They have a wide range of potential applications in DNA analysis, genetic disease diagnosis, virus detection and forensic applications (Du et al., 2010; He et al., 2012; Jung et al., 2010). Various techniques such as electrochemistry (Akhavan et al., 2012; Wang et al., 2013), electrochemiluminescence (Wang et al., 2008b), fluorescence (Ju et al., 2012), and quartz crystal microbalance (Fei et al., 2011) have been developed for DNA quantitative assay. Thereinto, electrochemistry is a promising strategy thanks to its high sensitivity, low cost and great

* Corresponding author. Tel.: +86 21 66134734.
E-mail address: luck@shu.edu.cn (L. Luo).

http://dx.doi.org/10.1016/j.bios.2014.03.067
0956-5663/

potential for on-site testing (Akhavan et al., 2012; Liu et al., 2013; Wang et al., 2013).

Electrochemical impedance spectroscopy (EIS) is an efficient and powerful tool for biorecognition interface study of biosensor (Wang et al., 2012). The biorecognition layer on electrode surface is of crucial importance for impedance measurement. To construct electrochemical biosensors with high sensitivity and selectivity, transducing materials need to possess characteristics such as high conductivity, low electron transfer resistance, large specific surface area and excellent biocompatibility (Bonanni et al., 2012). Hybrid material based on graphene is an ideal platform that fulfils all these requirements to prepare electrochemical impedance DNA biosensors. Chen et al. (2011a), have demonstrated a convenient enzyme-assisted signal amplification strategy based on a graphene/gold nano-particles modified electrode for the detection of DNA target by EIS. Hu et al. (2012) have constructed an efficient DNA impedance biosensing platform based on N,N-bis-(1-aminopropyl-3-propylimidazol salt)-3,4,9,10-perylene tetracarboxylic acid diimide/graphene for selectively detecting the conserved sequence of the pol gene of HIV-1. Bonanni and Pumera (2011) have investigated several electrochemical EIS platforms based on different numbers of same-sized graphene layers for rapid detection of single nucleotide polymorphisms correlated to Alzheimer's disease.

Herein, a novel label-free electrochemical impedance DNA biosensor with high sensitivity and specificity has been fabricated based on TRA-functionalized rGO. The mild, low-cost and eco-friendly approach to non-covalent functionalization of rGO improves the stability and hydrophilicity of rGO and preserves its intrinsic properties of high specific surface area, good electrical conductivity and biocompatibility. TRA is chosen for preparing rGO hybrid and fabricating electrochemical impedance DNA biosensor because its indole ring with flat, hydrophobic face can stack onto the surface of rGO, and its amino group can be conjugated to amino-substituted oligonucleotide probe by cross-linker glutaraldehyde (GA). In addition, DNA hybridization reaction is monitored by EIS. The as-prepared electrochemical impedance DNA biosensor shows excellent reproducibility and provides potential applications in bioanalysis.

2. Experimental section

2.1. Reagents

Graphite oxide was obtained from Nanjing XFNANO Materials Tech Co. Ltd. (Nanjing, China). Hydrazine hydrate ($NH_2NH_2 \cdot H_2O$, 80%) was purchased from Aladdin (Shanghai, China). TRA and GA (25%) were provided by Sigma Co. (USA). KH_2PO_4, $K_2HPO_4 \cdot 3H_2O$, NaCl, $K_3Fe(CN)_6$ and $K_4Fe(CN)_6 \cdot 3H_2O$ were provided by Sinopharm Chemical Reagent Beijing Co. Ltd. Milli-Q water (18.25 MΩ cm) was used throughout the experiments. All synthetic oligonucleotide sequences were provided by Sangon Biotech Co. Ltd., (Shanghai, China). The sequences are as follows: the probe ssDNA (pDNA) is 5′-(NH_2-C_6)-AAT GTG CTC CCC CAA CTC CTC-3′; the complementary ssDNA (cDNA) from hepatitis B virus (HBV) sequence is 5′-GAG GAG TTG GGG GAG CAC ATT-3′ (Li et al., 2011); the one mismatch-containing ssDNA (c_1DNA) is 5′-GAG GAG TTG GAG GAG CAC ATT-3′; the non-complementary ssDNA (nDNA) is 5′-AAT GTG CTC CCC CAA CTC CTC-3′. The DNAs were dissolved in 50 mM Tris–HCl/0.1 M NaCl/0.2 M KCl/5 mM $MgCl_2$ (pH 7.4) buffer.

2.2. Instruments and characterizations

Tapping-mode atomic force microscopy (AFM) measurements were performed on an Agilent 5500 (USA) using a tapping mode. High resolution transmission electron microscopy (HR-TEM) images were obtained using a JEM-2010F transmission electron microscope (Japan, at an acceleration voltage of 200 kV). Raman scattering measurements were carried out on an InVia Raman microscope (Renishaw, UK) with an excitation laser wavelength of 514.5 nm. Fluorescence emission spectra were recorded using an RF-5301PC spectrofluorometer with an excitation wavelength of 249.0 nm in a 1-cm quartz cell. Both excitation and emission slit widths were 3.0 nm. Cyclic voltammetry (CV) measurements were performed on a CHI 660D electrochemical workstation (Shanghai CH Instrument Co., China). EIS measurements were tested by a Solartron 1255B Frequency Response Analyzer/SI 1287 Electrochemical Interface (Scribner Associates, Inc.) using 5 mM $[Fe(CN)_6]^{3-/4-}$ as the electrochemical probe. A conventional three-electrode system was used with a saturated calomel electrode as the reference electrode, a platinum sheet as the counter-electrode, and a modified glassy carbon electrode (GCE, $\Phi = 1$ mm) as the working electrode. 5 mV amplitude of sine voltage signal was applied to the three-electrode system under open circuit potential, and frequency varied from 0.1 Hz to 100 kHz.

2.3. Preparation of rGO and TRA–rGO

RGO was prepared according to the literature (Zhu et al., 2012). First, graphite oxide dispersion (5 mg graphite oxide was dispersed in 50 mL water) was exfoliated by sonicating under ambient conditions for 40 min. The dispersion was centrifuged at 3000 rpm for 5 min to obtain claybank supernatant, namely graphene oxide (GO) dispersion. Subsequently, $NH_2NH_2 \cdot H_2O$ (1% v/v) was added into the GO solution, and the resulting mixture was heated to 100 °C and kept stirring for 24 h. Then, the above solution was filtered, and the filtration residue was dried to obtain black rGO powder under vacuum at 60 °C. Finally, the obtained product (rGO) was stored under ambient condition.

TRA–rGO was prepared as follows. 10 mg rGO and 20 mg TRA were dispersed in 30 mL ethanol, and the dispersion was treated with continuous sonicating for 1 h and then mechanical stirring for 24 h at room temperature. The obtained black dispersion was centrifuged and rinsed with ethanol three times to get dark centrifugation residue. Finally, the product (TRA–rGO) was dried in a vacuum drying oven at 70 °C for 0.5 h and collected for further use.

2.4. Fabrication of electrochemical impedance DNA biosensor

Prior to surface modification, GCE was polished carefully with 1.0, 0.3 and 0.05 μm alumina powder successively to obtain a mirror-shiny surface. The polished GCE was cleaned sequentially with 1:1 HNO_3, ethanol and water under continuous sonication for 3 min, respectively. Afterwards, the GCE was continuously scanned within a potential range of −1.0 V to +1.0 V in freshly prepared deoxygenated 0.5 M H_2SO_4 for 15 cycles to activate its surface. Finally, the GCE was allowed to dry under a stream of high purity nitrogen for further use.

TRA–rGO was dispersed in 0.5% (wt/wt) GA solution to form homogeneous black ink-like GA–TRA–rGO suspension (1 mg mL^{-1}) under ultrasonic vibration for 30 min. Then, the suspension was diluted with ethanol to obtain 0.67 mg mL^{-1} GA–TRA–rGO dispersion. 6 μL of the prepared dispersion was dropped onto the GCE surface and dried under an infrared lamp for 20 min to form GA–TRA–rGO/GCE. The GA–TRA–rGO/GCE was rinsed with deionized water and dried under an N_2 stream. Subsequently, 10 μL of 5 μM pDNA was dropped onto the surface of the GA–TRA–rGO/GCE, and incubated for 2 h at 35 °C to obtain pDNA/GA–TRA–rGO/GCE. Finally, the pDNA/GA–TRA–rGO/GCE was rinsed carefully with 0.1 M PBS + 0.01 M NaCl (pH 7.0), dried under an N_2 stream and stored at 4 °C for further use.

2.5. Hybridization and electrochemical measurements of the DNA biosensor

10 μL analyte solution (cDNA, c_1DNA or nDNA) with desired concentration was dropped onto the surface of pDNA/GA–TRA–rGO/GCE and incubated for 40 min at 35 °C. Afterwards, the hybridized electrode was rinsed with 0.1 M PBS+0.01 M NaCl (pH 7.4) to remove the non-specifically adsorbed target DNAs. After hybridization reaction, the obtained electrodes were denoted as cDNA–pDNA/GA–TRA–rGO/GCE, c_1DNA–pDNA/GA–TRA–rGO/GCE and nDNA–pDNA/GA–TRA–rGO/GCE, correspondingly.

3. Results and discussion

3.1. Fabrication of TRA–rGO-based DNA biosensor

A schematic diagram of electrochemical impedance DNA biosensor is displayed in Scheme 1. TRA with the planar configuration was stacked onto rGO surface via π-stacking interaction. To fabricate electrochemical impedance DNA biosensor, an amino-substituted oligonucleotide probe was conjugated to the amino group of TRA by GA.

3.2. Characterizations of rGO and TRA–rGO

Morphologies of rGO and TRA–rGO were characterized by AFM and HR-TEM, as shown in Fig. 1. The samples for AFM were prepared by dip-coating rGO and TRA–rGO dispersions onto freshly-cleaved mica. Fig. 1A indicates a typical cross-section picture of well-exfoliated rGO. The thickness of rGO is ~0.9 nm, which is consistent with the characteristic value reported in the literature (Li et al., 2008). When rGO is non-covalently functionalized with TRA, the thickness of a single layer TRA–rGO is ~1.7 nm (Fig. 1B). It is reasonable that TRA molecules cover both sides of rGO sheet with face-to-face orientation in a sandwich-like manner via π-stacking interaction, and then it is deduced that the interlayer distance between TRA and rGO is ~0.4 nm (Su et al., 2009; Chen et al., 2011b), which corresponds to theoretical study of the interaction between tryptophan (a close analog of TRA) and graphene by Rajesh et al. (2009). Besides single-layer TRA–rGO, the AFM image also shows that certain TRA molecules aggregate somewhere on rGO surface (the golden dots). This may be due to the fact that residual oxygen-containing functional groups on the basal plane of rGO can also absorb TRA molecules via hydrogen bonding interaction, which is similiar to aggregation of 1-aminopyrene on graphene surface (Kubota et al., 2011; Matsumoto et al., 2002).

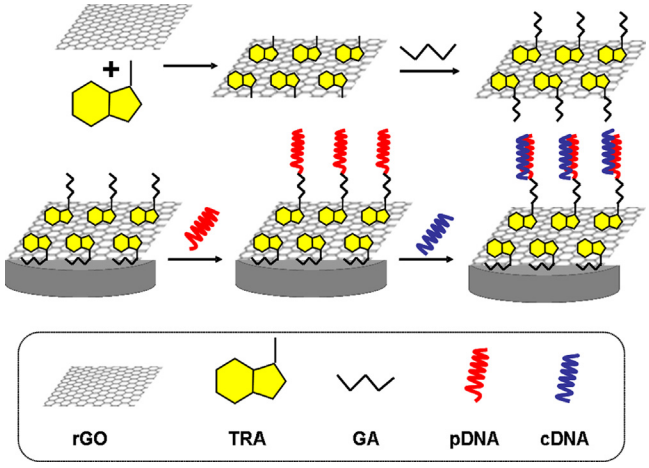

Scheme 1. Schematic diagram of the electrochemical impedance DNA biosensor.

HR-TEM is a powerful tool which can provide imaging information of graphene sample down to mono-atomic thickness level (Robertson and Warner, 2013). Fig. 1C shows morphology of rGO with a typical wrinkled structure, while Fig. 1D illustrates that TRA molecules are widely distributed on the rGO sheet, and that TRA aggregates are 10–50 nm in diameter, which is consistent with that of the AFM image (Fig. 1B).

Raman spectroscopy has been widely used for the characterization of carbon products, considering the fact that conjugated carbon–carbon double bonds lead to high Raman intensities (Feng et al., 2012). The powdery samples of GO, rGO and TRA–rGO were studied by Raman spectroscopy (Fig. S1A, Supplementary information). The spectrum of GO (curve a in the inset) exhibits two peaks at 1379 and 1606 cm^{-1} ascribed to D and G bands, respectively. The D band is associated with the disorder, defect and edge of carbons in graphene, while the G band arises from the first order scattering of the E_{2g} phonon of sp^2 carbon hybridization (Xie et al., 2012). The position of the two bands indicates that GO lies between crystalline and nano-crystalline sp^2 carbon from the Ferrari amorphization trajectory (Panigrahi et al., 2011). After GO is reduced to rGO (curve b in the inset), both D and G bands downshift to 1332 and 1581 cm^{-1} (Wu et al., 2012), respectively. The shift of D band from 1379 to 1332 cm^{-1} may be ascribed to the reduction of GO. Meanwhile, the D/G intensity ratio of rGO (I_D/I_G=1.42) increases compared with that of GO (1.03), suggesting the increase of rGO defects (Akhavan et al., 2012). The I_D/I_G can also be used to estimate crystalline size (*La*) of rGO. According to the empirical Tuinstra–Koening relation *La* (in nm)=$(2.4\times10^{-10})\lambda_4(I_D/I_G)^{-1}$, where λ is the Raman excitation wavelength (λ=514.5 nm) (Tuinstra and Koenig, 1970), the average sizes of the sp^2 domains of GO and rGO are estimated to be 16.31 and 11.83 nm, respectively. The smaller *La* of rGO illustrates that its electrical resistivity is superior to that of GO owing to the hopping of carriers between crystallites in the sample (Pimenta et al., 2007). After the non-covalent functionalization of rGO by TRA, the intensity of D, G, D′ and G′ bands of TRA–rGO (curve d) is ~1.5 times than that of rGO, and the D/G intensity ratio of TRA–rGO decreases to ~1.30 under the same conditions, which provides further evidence on the interaction between rGO and TRA while the band positions of TRA–rGO have not changed, suggesting that the structure of rGO is not destroyed by the adsorption of TRA molecules (Gong et al., 2008).

Fluorescence spectroscopy was performed to study π-stacking interaction between TRA and rGO. Fig. S1B (see Supplementary information) shows the fluorescence spectra of rGO (inset), TRA (curve *c*) and TRA–rGO (curve *d*). The TRA spectrum exhibits a broad fluorescence band at around 363.0 nm. After TRA was attached onto rGO surface by π-stacking interaction, its fluorescence was significantly quenched. The high efficiency fluorescence quenching is due to the fact that planar configurations of rGO and TRA guarantee their close proximity, which is beneficial for the fluorescence resonance energy transfer (Kong et al., 2011). The results demonstrate the successful non-covalent binding between TRA and rGO.

3.3. Electrochemical characterization of different electrodes

In order to characterize electrochemical properties of different electrodes, CV and EIS were performed in 0.1 M PBS (pH 7.4)+0.01 M NaCl+5 mM $Fe(CN)_6^{3-/4-}$ (1:1). As shown in Fig. S2A (see Supplementary information), the peak current of $[Fe(CN)_6]^{3-/4-}$ at GA–TRA–rGO/GCE is lower than that at bare GCE, and the potential difference of $[Fe(CN)_6]^{3-/4-}$ between anodic peak and cathodic peak at GA–TRA–rGO/GCE becomes larger (curve *b*) compared

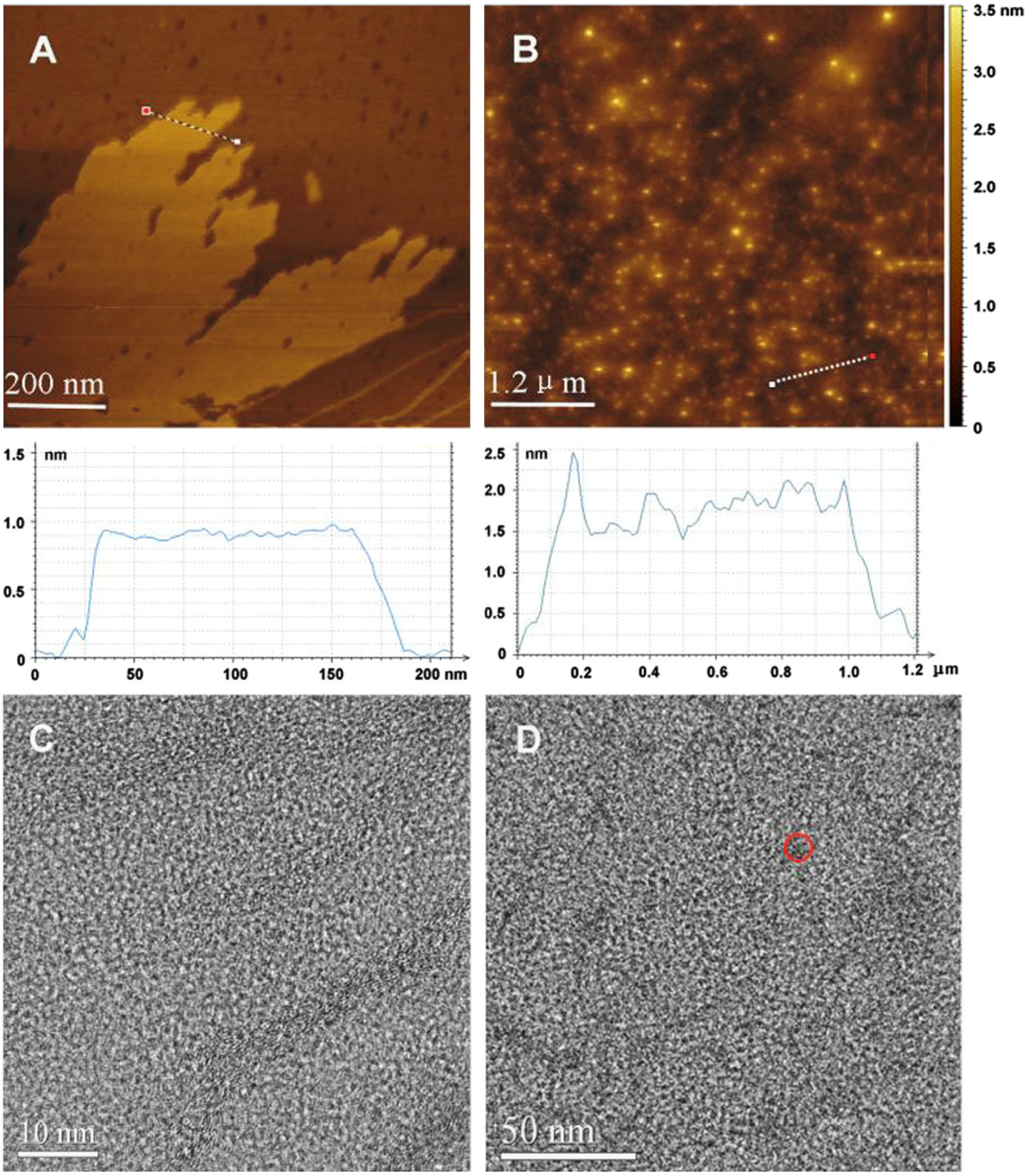

Fig. 1. Tapping-mode AFM images and cross-section graphs of rGO (A) and TRA–rGO (B) dispersion dip-coated on mica; HR-TEM micrographs of rGO (C) and TRA–rGO (D). (For interpretation of the references to color in this figure, the reader is referred to the web version of this article.)

with that at bare GCE (curve a), suggesting that the electrochemical redox reversibility of $[Fe(CN)_6]^{3-/4-}$ at GA–TRA–rGO/GCE becomes poorer. When pDNA was covalently attached to the GA–TRA–rGO/GCE, an obvious decrease of the redox peak current of $[Fe(CN)_6]^{3-/4-}$ (curve c) is observed because negative charges of phosphoric acid groups on the pDNA interfere with the diffusion of electronegative $[Fe(CN)_6]^{3-/4-}$ to the electrode surface (Xu et al., 2012). After the hybridization reaction of cDNA, the peak current of $[Fe(CN)_6]^{3-/4-}$ at cDNA/pDNA/GA–TRA–rGO/GCE (curve d) decreases further.

EIS has been proved as a powerful tool for sensitive study of biorecognition events on electrode surface (Bonanni et al., 2012; Wang, 2008c). Fig. S2B (see Supplementary information) shows Nyquist diagrams of different modified electrodes. In Nyquist diagrams, the semicircle portion at higher frequencies relates to the electron-transfer-limited process, while the linear part at lower frequencies corresponds to the diffusion process. Increase in semicircle diameter reflects the increase in interfacial electron-transfer resistance (R_{et}). After GCE is modified with GA–TRA–rGO, the R_{et} value increases from 0 Ω (curve a) to 780.0 Ω (curve b), which is due to the fact that the long carbon chain of GA blocks electron transfer of the redox probe $[Fe(CN)_6]^{3-/4-}$ to electrode surface. The R_{et} value of pDNA/GA–TRA–rGO/GCE increases to 1341.5 Ω (curve c) compared with that of GA–TRA–rGO/GCE. When pDNA/GA–TRA–rGO/GCE is hybridized with 10^{-9} M cDNA, the R_{et} value of cDNA/pDNA/GA–TRA–rGO/GCE increases further to 1775.3 Ω (curve d). R_{et} is continually increased because the electron transfer of $[Fe(CN)_6]^{3-/4-}$ is restrained by electrostatic

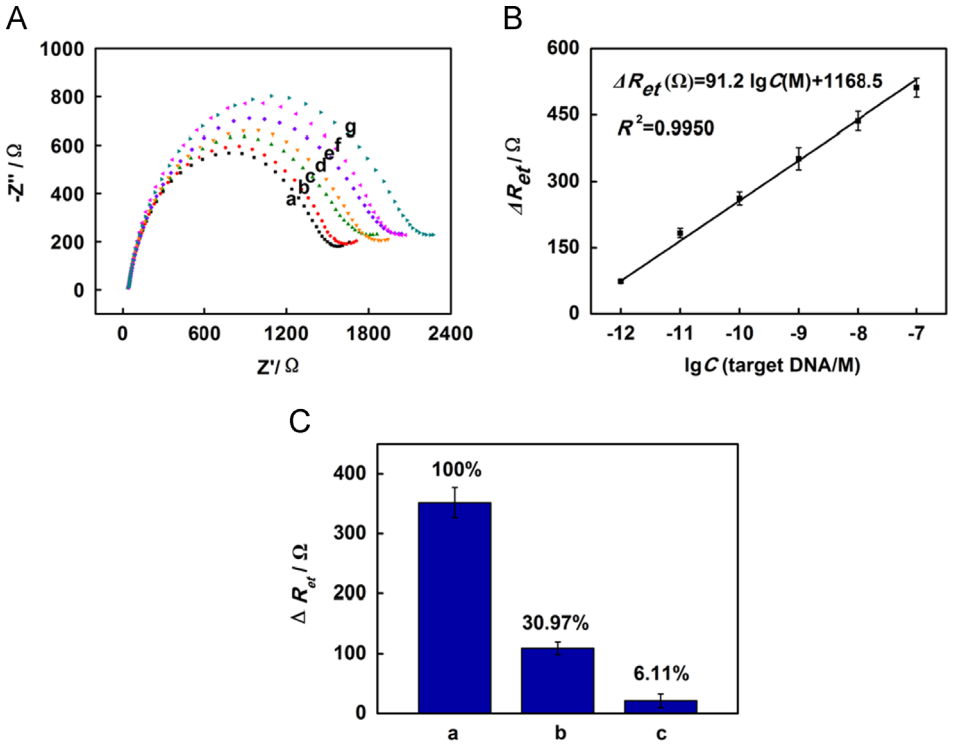

Fig. 2. (A) Nyquist diagrams of pDNA/GA–TRA–rGO/GCE hybridization with different concentrations of cDNA: 0, 1.0×10^{-12}, 1.0×10^{-11}, 1.0×10^{-10}, 1.0×10^{-9}, 1.0×10^{-8} and 1.0×10^{-7} M (a→g). (B) Corresponding data analysis of (A). (C) ΔR_{et} of 1 nM cDNA/pDNA/GA–TRA–rGO/GCE (a), c_1DNA/pDNA/GA–TRA–rGO/GCE (b), and nDNA/pDNA/GA–TRA–rGO/GCE (c). The electrochemical detection was in 0.1 M PBS (pH 7.4)+0.01 M NaCl+5 mM $Fe(CN)_6^{3-/4-}$ (1:1). The number of replicates is three, and error bars correspond to R.S.D. of ΔR_{et} value. The frequency varied from 0.1 Hz to 100 kHz, and 5 mV amplitude of sine voltage signal was used.

repulsion of the negatively charged phosphoric acid groups of DNA strands on electrode surface. The results of EISs here are consistent with those of CVs in Fig. S2A.

3.4. Label-free oligonucleotides detection with proposed impedance DNA biosensors

After cDNA hybridization reaction at pDNA/GA–TRA–rGO/GCE, the R_{et} value of cDNA/pDNA/GA–TRA–rGO/GCE increases with increasing cDNA concentration due to the restrained electron transfer of $[Fe(CN)_6]^{3-/4-}$ to electrode surface. The difference between R_{et} value (ΔR_{et}) of cDNA/pDNA/GA–TRA–rGO/GCE and that of pDNA/GA–TRA–rGO/GCE is adopted as the measurement signal, i.e., $\Delta R_{et}=R_{et,cDNA}-R_{et,pDNA}$.

Under optimized experimental conditions (pDNA/GA–TRA–rGO/GCE is hybridized with cDNA at 35 °C for 40 min, as shown in Fig. S4 in the Supplementary information), ΔR_{et} increases linearly with increasing cDNA concentration from 1.0×10^{-12} M to 1.0×10^{-7} M with the regression equation $\Delta R_{et}(\Omega)=91.2\ \lg C\ (M)+1168.5$ and correlation coefficient of 0.9950 (Fig. 2A and B). The detection limit is estimated to be 5.2×10^{-13} M with 3σ (where σ is the relative standard deviation of 11 parallel measurements of the blank solution). The simple and cost-effective electrochemical impedance DNA sensor based on TRA–rGO has excellent sensitivity and wide dynamic range compared with our former research and other literatures (Table S1, Supplementary information).

3.5. Specificity and reproducibility of the electrochemical impedance biosensor

Individual variations in the human genome have drawn considerable attention recently (Shi et al., 2011). It is important to develop fast, sensitive, and cost-effective methods for identifying point mutations in DNA sequences. In the experiment, we studied a simple case for point mutations recognition in which cDNA, c_1DNA (oligonucleotide with a single base mutation) and nDNA were hybridized with pDNA. As shown in Fig. 2C, hybridization reaction is effective only with cDNA; for instance, ΔR_{et} values of c_1DNA/pDNA/GA–TRA–rGO/GCE and nDNA/pDNA/GA–TRA–rGO/GCE are 30.97% and 6.11% of cDNA/pDNA/GA–TRA–rGO/GCE, respectively. The experimental results indicate that the electrochemical impedance DNA biosensor has excellent specificity.

To evaluate reproducibility of the label-free impedance DNA biosensor, three trials were run, using pDNA/GA–TRA–rGO/GCEs from several batches prepared on different days. The pDNA/GA–TRA–rGO/GCEs were hybridized with 1 nM cDNA under the optimized experimental conditions. A satisfying relative standard deviation (R.S.D.) of 7.7% ($n=3$) for ΔR_{et} value was estimated, showing that the impedance DNA biosensor has high reproducibility.

4. Conclusion

A simple and effective label-free electrochemical impedance biosensor based on TRA–rGO has been developed for sensitive determination of DNA with high specificity by monitoring ΔR_{et} caused by DNA hybridization reaction. In our approach, TRA is used to non-covalently functionalize rGO based on π-stacking interaction. The non-covalent functionalization strategy can improve the stability and hydrophilicity of rGO and preserve its intrinsic properties of high specific surface area, good electrical conductivity and biocompatibility. As proof-of-principle experiments, complementary DNA detection of 21-mer oligonucleotide (based on the hepatitis B virus sequence) has been carefully studied. The experimental results demonstrate that our approach can serve as a low-cost technique for genetic studies.

Acknowledgments

The authors would like to thank the National Natural Science Foundation of China (Nos. 21271127 and 61171033) and the Nano-Foundation of Science and Techniques Commission of Shanghai Municipality (Nos. 12nm0504200 and 12dz1909403) for financial supports.

Appendix A. Supporting information

Supplementary data associated with this article can be found in the online version at http://dx.doi.org/10.1016/j.bios.2014.03.067.

References

Artiles, M.S., Rout, C.S., Fisher, T.S., 2011. Adv. Drug Deliv. Rev. 63, 1352–1360.
Akhavan, O., Ghaderi, E., Rahighi, R., 2012. ACS Nano 6, 2904–2916.
Bonanni, A., Pumera, M., 2011. ACS Nano 5, 2356–2361.
Bonanni, A., Loo, A.H., Pumera, M., 2012. Trends Anal. Chem. 37, 12–21.
Chen, Y., Jiang, B.Y., Xiang, Y., Chai, Y.Q., Yuan, R., 2011a. Chem. Commun. 47, 12798–12800.
Chen, C., Zhai, W.T., Lu, D.D., Zhang, H.B., Zheng, W.G., 2011b. Mater. Res. Bull. 46, 583–587.
Chen, I.-W.P., 2013. Chem. Commun. 49, 2753–2755.
Du, M., Yang, T., Jiao, K., 2010. J. Mater. Chem. 20, 9253–9260.
Dutta, S., Pati, S.K., 2010. J. Mater. Chem. 20, 8207–8223.
Fei, Y.H., Jin, X.Y., Wu, Z.S., Zhang, S.B., Shen, G.L., Yu, R.Q., 2011. Anal. Chim. Acta 691, 95–102.
Feng, H.B., Li, Y.M., Li, J.H., 2012. RSC Adv. 2, 6988–6993.
Gong, M.J., Han, T., Cai, C.X., Lu, T.H., Du, J.Y., 2008. J. Electroanal. Chem. 623, 8–14.
Ghosh, A., Rao, K.V., George, S.J., Rao, C.N.R., 2010. Chem. Eur. J. 16, 2700–2704.
He, S.J., Liu, K.K., Su, S., Yan, J., Mao, X.H., Wang, D.F., He, Y., Li, L.J., Song, S.P., Fan, C.H., 2012. Anal. Chem. 84, 4622–4627.
Hayama, T., Sakaguchi, Y., Yoshida, H., Itoyama, M., Todoroki, K., Yamaguchi, M., Nohta, H., 2012. Anal. Chem. 84, 8407–8414.
Hu, Y.W., Wang, K.K., Zhang, Q.X., Li, F.H., Wu, T.S., Niu, L., 2012. Biomaterials 33, 1097–1106.
Jung, J.H., Cheon, D.S., Liu, F., Lee, K.B., Seo, T.S., 2010. Angew. Chem. Int. Ed. 49, 5708–5711.
Ju, E.G., Yang, X.J., Lin, Y.H., Pu, F., Ren, J.S., Qu, X.G., 2012. Chem. Commun. 48, 11662–11664.
Kubota, S., Maruyama, T., Nishikiori, H., Ito, F., Tanaka, N., Endo, M., Fujii, T., 2011. J. Photochem. Photobiol. A 218, 226–230.
Kong, L.T., Wang, J., Zheng, G.C., Liu, J.H., 2011. Chem. Commun. 47, 10389–10391.
Li, D., Müller, M.B., Gilje, S., Kaner, R.B., Wallace, G.G., 2008. Nat. Nanotechnol. 3, 101–105.
Li, F., Feng, Y., Dong, P.J., Yang, L.M., Tang, B., 2011. Biosens. Bioelectron. 26, 1947–1952.
Liu, J., Tang, J., Gooding, J.J., 2012. J. Mater. Chem. 22, 12435–12452.
Liu, Y.H., Li, H.N., Chen, W., Liu, A.L., Lin, X.H., Chen, Y.Z., 2013. Anal. Chem. 85, 273–277.
Lin, C.T., Loan, P.T.K., Chen, T.Y., Liu, K.K., Chen, C.H., Wei, K.H., Li, L.J., 2013. Adv. Funct. Mater. 23, 2301–2307.
Matsumoto, H., Koyama, Y., Tanioka, A., 2002. Langmuir 18, 3698–3703.
Meyer, J.C., Geim, A.K., Katsnelson, M.I., Novoselov, K.S., Booth, T.J., Roth, S., 2007. Nature 446, 60–63.
Novoselov, K.S., Geim, A.K., Morozov, S.V., Jiang, D., Zhang, Y., Dubonos, S.V., Grigorieva, I.V., Firsov, A.A., 2004. Science 306, 666–669.
Pimenta, M.A., Dresselhaus, G., Dresselhaus, M.S., Cançado, L.G., Jorio, A., Saito, R., 2007. Phys. Chem. Chem. Phys. 9, 1276–1290.
Panigrahi, S., Bhattacharya, A., Bandyopadhyay, D., Grabowski, S.J., Bhattacharyya, D., Banerjee, S., 2011. J. Phys. Chem. C 115, 14819–14826.
Premkumar, T., Geckeler, K.E., 2012. Prog. Polym. Sci. 37, 515–529.
Pham, H.V., Martin, D.B.C., Vanderwal, C.D., Houk, K.N., 2012. Chem. Sci. 3, 1650–1655.
Ramanathan, T., Abdala, A.A., Stankovich, S., Dikin, D.A., Herrera-Alonso, M., Piner, R.D., Adamson, D.H., Schniepp, H.C., Chen, X., Ruoff, R.S., Nguyen, S.T., Aksay, I. A., Prud'Homme, R.K., Brinson, L.C., 2008. Nat. Nanotechnol. 3, 327–331.
Rao, C.N.R., Sood, A.K., Subrahmanyam, K.S., Govindaraj, A., 2009. Angew. Chem. Int. Ed. 48, 7752–7777.
Rajesh, C., Majumder, C., Mizuseki, H., Kawazoe, Y., 2009. J. Chem. Phys. 130, 124911–124916.
Robertson, A.W., Warner, J.H., 2013. Nanoscale 5, 4079–4093.
Su, Q., Pang, S.P., Alijani, V., Li, C., Feng, X.L., Müllen, K., 2009. Adv. Mater. 21, 3191–3195.
Sun, Z.Z., Kohama, S.I., Zhang, Z.X., Lomeda, J.R., Tour, J.M., 2010. Nano Res. 3, 117–125.
Shi, C., Zhao, C.H., Guo, Q.J., Ma, C.P., 2011. Chem. Commun. 47, 2895–2897.
Tuinstra, F., Koenig, J.L., 1970. J. Chem. Phys. 53, 1126–1130.
Tang, J., Hou, L., Tang, D.P., Zhou, J., Wang, Z.P., Li, J.R., Chen, G.N., 2012. Biosens. Bioelectron. 38, 86–93.
Wang, S.Y., Wang, X., Jiang, S.P., 2008a. Langmuir 24, 10505–10512.
Wang, X.Y., Yun, W., Dong, P., Zhou, J.M., He, P.G., Fang, Y.Z., 2008b. Langmuir 24, 2200–2205.
Wang, J.X., 2008c. Phys. Rev. B 78, 245304.
Wen, Y.Q., Peng, C., Li, D., Zhuo, L., He, S.J., Wang, L.H., Huang, Q., Xu, Q.H., Fan, C.H., 2011. Chem. Commun. 47, 6278–6280.
Wang, D., Li, Y.G., Hasin, P., Wu, Y.Y., 2011. Nano Res. 4, 124–130.
Wu, P., Qian, Y.D., Du, P., Zhang, H., Cai, C.X., 2012. J. Mater. Chem. 22, 6402–6412.
Wang, Y.P., Xiao, Y.H., Ma, X.L., Li, N., Yang, X.D., 2012. Chem. Commun. 48, 738–740.
Wang, Q.B., Lei, J.P., Deng, S.Y., Zhang, L., Ju, H.X., 2013. Chem. Commun. 49, 916–918.
Xu, Y.X., Bai, H., Lu, G.W., Li, C., Shi, G.Q., 2008. J. Am. Chem. Soc. 130, 5856–5857.
Xu, H.F., Wang, L.L., Ye, H.Z., Yu, L.S., Zhu, X., Lin, Z.Y., Wu, G.W., Li, X.H., Liu, X.X., Chen, G.N., 2012. Chem. Commun. 48, 6390–6392.
Xie, Y.Q., McAllister, S.D., Hyde, S.A., Sundararajan, J.P., FouetioKengne, B.A., McIlroy, D.N., Cheng, I.F., 2012. J. Mater. Chem. 22, 5723–5729.
Yang, S.B., Feng, X.L., Wang, X.C., Müllen, K., 2011. Angew. Chem. Int. Ed. 50, 5339–5343.
Zhang, D.D., Fu, L., Liao, L., Liu, N., Dai, B.Y., Zhang, C.X., 2012. Nano Res. 5, 875–887.
Zhu, L.M., Luo, L.Q., Wang, Z.X., 2012. Biosens. Bioelectron. 35, 507–511.